applied optics

Design and fabrication of a Fresnel zone plate with an enhanced depth of focus

Hieu Tran Doan Trung,[1,2] Hai Linh Vu Nguyen,[1,2] Atar Munnibee,[1,2] Young-Jin Kim,[3] Young-Sik Ghim,[1,2,4] and Hyug Gyo Rhee[1,2,*]

[1]Department of Science of Measurement, University of Science and Technology (UST), Daejeon 34113, Republic of Korea
[2]Length and Dimensional Metrology Group, Physical Metrology Division, Korea Research Institute of Standards and Science (KRISS), Daejeon 34113, Republic of Korea
[3]Department of Mechanical Engineering, Korea Advanced Institute of Science and Technology (KAIST), Daejeon 34141, Republic of Korea
[4]young.ghim@kriss.re.kr
*hrhee@kriss.re.kr

Received 30 May 2024; revised 26 July 2024; accepted 30 July 2024; posted 31 July 2024; published 14 August 2024

A Fresnel zone plate (EFZP) with an extended depth of focus can maintain focused monochromatic light at different distances compared to a general Fresnel zone plate (FZP). The focal distances are determined by dividing the zone plate into multiple areas based on the desired order. The EFZP has potential applications in various research fields such as microscopy, direct laser lithography, and optical coherence tomography. However, manufacturing an EFZP is challenging due to the high precision requirements and difficulties associated with the calculation and simulation processes. In this research, a complete process is presented to design, simulate, and fabricate an EFZP using a Fourier optics design, simulations, and a direct laser lithographic machine. The resulting EFZP has an increased depth of focus of about nine times compared to a general Fresnel zone plate with similar parameters, while maintaining the focal spot diameter. The performance of this EFZP is evaluated through optical verification and mathematical simulation methods.

https://doi.org/10.1364/AO.531033

1. INTRODUCTION

The FZP is a well-known diffractive optics element that finds various applications in the field of optics such as computer-generated holograms [1–3], software testing, and even photography. One of the most impressive features of a FZP is its capability to function efficiently in short-wavelength light, such as X-rays [4,5], gamma rays [6,7], and ultraviolet rays [8,9], which distinguishes it from a lens. Therefore, the FZP plays a crucial role in not only the optics research field but also the optics industry.

In the photography and optics field, the depth of focus and depth of field are two distinct concepts. The depth of focus is the distance that the image plane moves along the optical axis while acceptably maintaining the sharpness. Meanwhile, the depth of field is the space between the farthest and the nearest objects that are in sharp focus. Some optical systems require a large depth of focus or depth of field, such as those used in laser ablation [10,11], microscopy [11,12], and machine vision lenses [13]. In this research work, we develop a method that can extend the depth of focus (DoF) of FZPs. Previous research papers have proposed various solutions to overcome the short focal length distance of FZPs. Some researchers have modified the FZP pattern and added additional equipment to the optics system to achieve the desired DoF. For instance, Zhang *et al*. used a fractal zone plate and one lens [14,15], while Xu *et al*. combined a multiring pure-phase FZP and a single lens [16]. Similarly, Torcal–Milla *et al*. used a sector-based FZP combined with a spatial light modulator (SLM) and two lenses to achieve a larger DoF [17].

However, these studies still have some limitations. For example, the concept of a fractal zone plate [14,15] or a multiring pure-phase FZP [16] may result in a loss of intensity due to the large opaque area, especially when relatively few stages are used. Additionally, using a lens to focus the light from the zone plate can cause certain optical aberrations. Moreover, the concept of the sector-based zone plate in earlier work [17] requires multiple optical elements in the system, such as a SLM with a beam splitter, two lenses, a pinhole, a quarter-wave plate, and a phase map to remove the aberrations of the wavefront. Moreover, using a SLM to implement a zone plate pattern can pose additional challenges when fabricating patterns with small parameters [18] or, in [19], the three-dimensional finite-difference time domain algorithm is applied to evaluate the optics performance but has not fabricated the real product making it difficult to use in the industrial field.

To address these drawbacks, our research focuses on developing a method of designing and manufacturing an EFZP that does not require any external optical equipment, while the EFZP is in use. Thus, we divided the FZP into multiple sub-areas with different focal lengths, allowing us easily to determine the order of the sub-areas and their focal length for specific purposes, such as extending the DoF or creating a zone plate with multiple focal lengths. The greatest challenge is the fabrication process due to the complexity of the FZP pattern and the small parameters involved. To overcome this challenge, the direct laser lithography method, which has been proven effective in previous research [20–22], especially in FZP manufacturing [23–25], is utilized. First, we calculate the EFZP by adjusting the ratio between each sub-area, after which we apply Fresnel propagation [26–28] to simulate its performance. The laser writing pattern is then generated to control the laser machine, and finally, a chemical etching method is used to form the EFZP. In order to prove the effectiveness of the EFZP, we conducted an experiment using an optical verification system.

The rest of this paper is structured as follows: Section 2 explains the design method of the EFZP; Section 3 demonstrates the simulation process; Section 4 explains the fabrication method; Section 5 presents the experiment; finally, Section 6 concludes the paper.

2. EFZP DESIGN PROCESS

The well-known transmittance function of the FZP in Fourier optics is based on the traditional design equation of creating alternating transparent and opaque regions [29]:

$$t_A(r) = \frac{1}{2}\left\{1 + \text{sign}\left[\cos\left(\frac{k}{2f}r^2\right)\right]\right\}\text{circ}\left(\frac{r}{w}\right), \quad (1)$$

whilst w is the radius of the zone plate of the FZP; $k = \frac{2\pi}{\lambda}$; λ is the wavelength, and f is the focal length of the zone plate; $r = \sqrt{x^2+y^2}$; and x and y are the coordinates of the sample matrix. The circle equation circ is given by

$$\text{circ}\left(\frac{r}{w}\right) = \begin{cases} 1 \text{ if } \left|\frac{r}{w}\right| \le 1 \\ 0 \text{ if } \left|\frac{r}{w}\right| > 1 \end{cases}, \quad (2)$$

and the purpose of the circle equation is to generate the circular shape of the zone plate. Moreover, the sign function necessary to form the binary zone plate is defined as follows:

$$\text{sign}\left(\left[\cos\left(\frac{k}{2f}r^2\right)\right]\right) = \begin{cases} 1 & \text{if } \left[\cos\left(\frac{k}{2f}r^2\right)\right] < 0 \\ 0 & \text{if } \left[\cos\left(\frac{k}{2f}r^2\right)\right] = 0 \\ -1 & \text{if } \left[\cos\left(\frac{k}{2f}r^2\right)\right] > 0 \end{cases}. \quad (3)$$

Subsequently, the binary zone plate with a diameter of $2w$ focuses the light with λ at focal length f [Fig. 1(a)]. In addition, by modifying some of the parameters in Eq. (1), other variants of the zone plate are generated. For example, upon a change of Eq. (1) to

$$t_A(\text{r}) = \frac{1}{2}\left\{1 - \text{sign}\left[\cos\left(\frac{k}{2f}r^2\right)\right]\right\}\text{circ}\left(\frac{r}{w}\right), \quad (4)$$

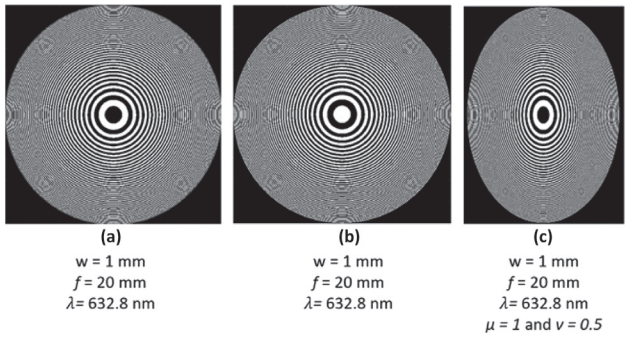

Fig. 1. (a) Negative binary zone plate, (b) positive binary zone plate, and (c) elliptical zone plate.

the zone plate will change from a negative zone plate to a positive zone plate [Fig. 1(b)]. Alternatively, if adding two constants μ and ν to adjust $r = \sqrt{\mu x^2+\nu y^2}$, the circular zone plate will turn into an elliptical zone plate [Fig. 1(c)].

As explained in the introduction, in order to create a multi-region zone plate with multiple focal lengths, the zone plate is divided into several sub-areas by adding a constant value (τ) to the equation (Eq. 1). For example, the first area of the multi-region zone plate can be defined as follows:

$$t_{A1}(r) = \frac{1}{2}\left\{1 - \text{sign}\left[\cos\left(\frac{k}{2f}r^2\right)\right]\right\}\text{circ}\left(\frac{r}{w}\tau_1\right), \quad \text{while } 0 < \tau_1 < 1. \quad (5)$$

Here the new zone with a radius equal to $w_1 = \tau_1 w$ is compared to the original zone plate. The next region t_{A2} with focal length f' and radius $w_2 = \tau_2 w$ is calculated by removing the inside area equal to $\tau_1 w$ so that the transmittance function of t_{A2} can then be calculated using the equation below:

$$t_{A2}(r) = \frac{1}{2}\left\{1 - \text{sign}\left[\cos\left(\frac{k}{2f'}r^2\right)\right]\right\}\text{circ}\left(\frac{r}{w}\tau_2\right) - \frac{1}{2}\left\{1 - \text{sign}\left[\cos\left(\frac{k}{2f'}r^2\right)\right]\right\}\text{circ}\left(\frac{r}{w}\tau_1\right)$$
$$\text{while } 0 < \tau_{1,2} < 1;\ \tau_1 < \tau_2;\ \tau_1+\tau_2 = 1. \quad (6)$$

The outcome here is a new zone plate with acreage identical to the original zone plate but with two focal lengths f and f'. In summary, the general formula to create a multi-region zone plate with radius w and m, focal lengths $f_1, f_2, f_3, \ldots f_m$, as well as $m+1$ constants $\tau_0, \tau_1, \tau_2, \tau_3 \ldots \tau_m$ is given by

$$t_A(r) = \sum_{m=1}^{m}\left\{\frac{1}{2}\left\{1 - \text{sign}\left[\cos\left(\frac{k}{2f_m}r^2\right)\right]\right\}\text{circ}\left(\frac{r}{w}\tau_m\right) - \frac{1}{2}\left\{1 - \text{sign}\left[\cos\left(\frac{k}{2f_m}r^2\right)\right]\right\}\text{circ}\left(\frac{r}{w}\tau_{m-1}\right)\right\}$$
$$\text{while } \tau_0 = 0;\ \tau_{m-1} < \tau_m,\ \tau_1, \tau_2, \tau_3 \ldots \tau_m > 1,$$
$$\sum_{m=1}^{m}\tau_m = 1. \quad (7)$$

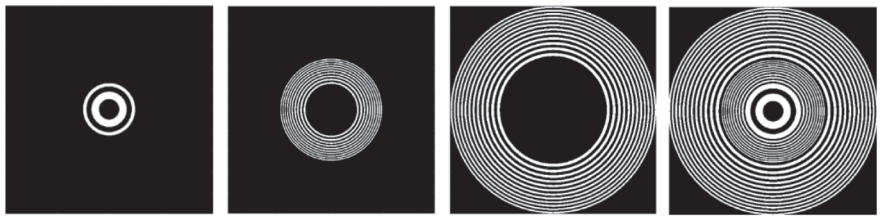

Fig. 2. Multi-focal-length Fresnel zone plate.

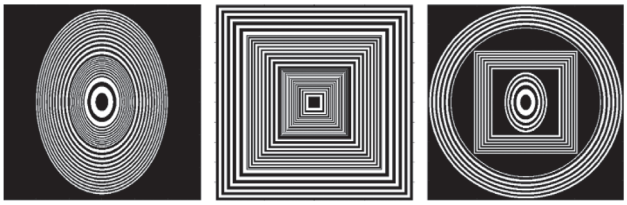

Fig. 3. Different types of multi-region zone plates: (a) multi-region elliptical zone plate, (b) multi-region square zone plate, and (c) combination of these three zone plate types.

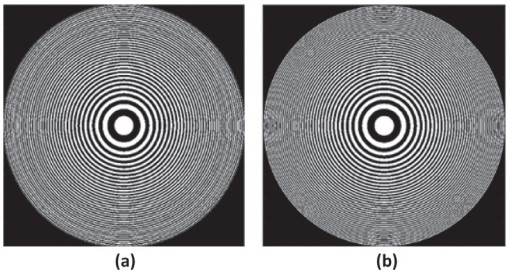

Fig. 4. (a) EFZP and (b) FZP simulation model.

As mentioned in the introduction, this concept is highly flexible. The acreage of each area, as well as the position of each focal length, can easily be arranged. This results in advantages when attempting to control the intensity of each focal length. Additionally, this design minimizes the opaque regions, unlike the fractal zone plate concept [14,15]. Figure 2 provides an example, showing a zone plate with three focal lengths of $f_1 = 30$ mm, $f_2 = 15$ mm, and $f_3 = 50$ mm with each zone having a different acreage with $\tau_1 = 0.25$, $\tau_2 = 0.5$, and $\tau_3 = 1$; the total radius $w = 1$ mm, and the wavelength $\lambda = 632.8$ nm.

Furthermore, many types of multi-region zone plates can be created, such as a multi-region elliptical zone plate [Fig. 3(a)], a multi-region square zone plate [Fig. 3(b)], and even a unique pattern that combines these three types of zone plates [Fig. 3(c)].

To increase the depth of field of a FZP, the gap between each focal length of the EFZP should be minimized. Depending on the number of regions, the focal length of the EFZP will be larger and smoother. The area of each region should also be considered to maintain the intensity of the EFZP. This paper presents the design of an EFZP to demonstrate its efficiency, as shown in Fig. 4(a). The EFZP will be simulated mathematically and verified through experiments in subsequent sections. In addition, a normal FZP, with similar parameters, will be used as a reference for comparison with the EFZP, as shown in Fig. 4(b).

Table 1. EFZP and FZP Parameters

	w (mm)	f (mm)	λ (nm)	τ_m
EFZP	1	20: 0.1: 22	632.8	$1/\sqrt{\frac{\alpha}{21}}$ while $\alpha = 1, 2, 3 \ldots 21$
FZP	1	21	632.8	

The EFZP has a radius of 1 mm and is divided into 21 regions with focal lengths ranging from 20 to 22 mm, with a gap of 0.1 mm between each focal length. Additionally, the wavelength used is $\lambda = 632.8$ nm, and each region has the same area. As a result, the total expected focal length of the EFZP ranges from 19.5 to 22.5 mm, which is a range of 3 mm. The parameters of this EFZP are illustrated in Table 1.

3. SIMULATION METHOD

Matlab software is used for the simulation process. The well-known Fresnel propagation equation is applied to describe the optical performance of the EFZP and FZP [30]:

$$U'(u, v) = \frac{e^{jkz}}{j\lambda z} \iint U(x, y)\, e^{\frac{jk}{2z}[(u-x)^2+(v-y)^2]} \mathrm{d}x\mathrm{d}y, \quad \textbf{(8)}$$

while $U'(u, v)$ is the propagation result of the source plane $U(u, v)$ at a distance of z (millimeters).The intensity chart is calculated a shown below [31]:

$$I(u, v) = \left|U'(u, v)\right|^2. \quad \textbf{(9)}$$

Equations (8) and (9) can simulate the optical performance of many diffractive elements. Figure 5 shows the simulation image and intensity result of a circular FZP, linear FZP, elliptical FZP, and square zone plate with the same focal length of 20 mm and wavelength $\lambda = 632.8$ nm. In a unique case such as the micro FZP, the numerical aperture of the FZP is bigger than 0.4; another method is suggested in [32–35].

Additionally, the image and intensity simulation results of the EFZP and FZP with a beam source $\lambda = 632.1$ nm and with a propagation distance ranging 19–25 mm are illustrated in Figs. 6 and 7 (see Visualization 1 and Visualization 2 for more details).

It is evident that the EFZP is more focused compared to the FZP. While the effective focal length of the FZP ranges from 20.5 to 21.5 mm (about 1 mm), the EFZP has a much larger range of 19–24.5 mm, resulting in a depth of field of about 5.5 mm, exceeding the expected DoF of 3 mm. In the next step, the process of fabricating the EFZP through direct laser lithography and chemical etching will be presented.

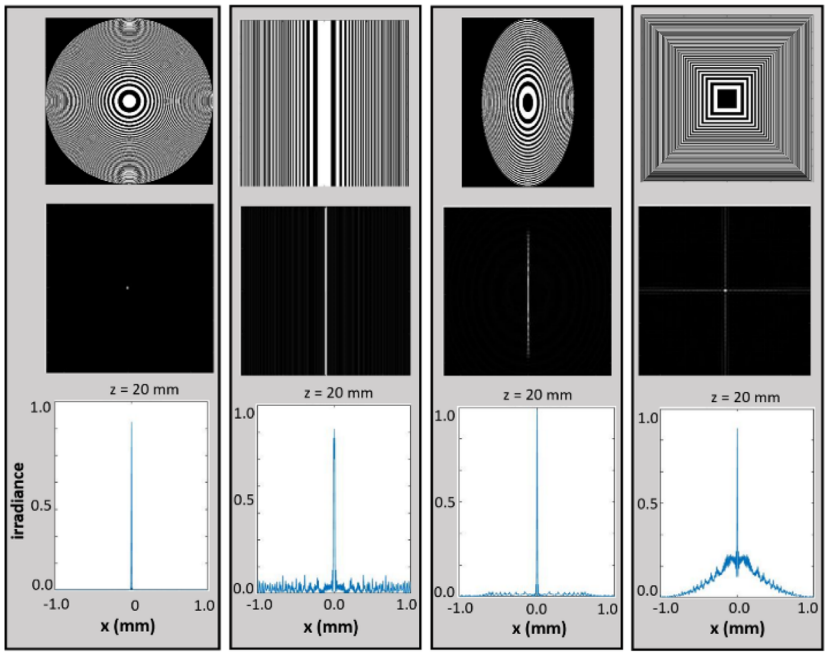

Fig. 5. Simulation results by Fresnel propagation.

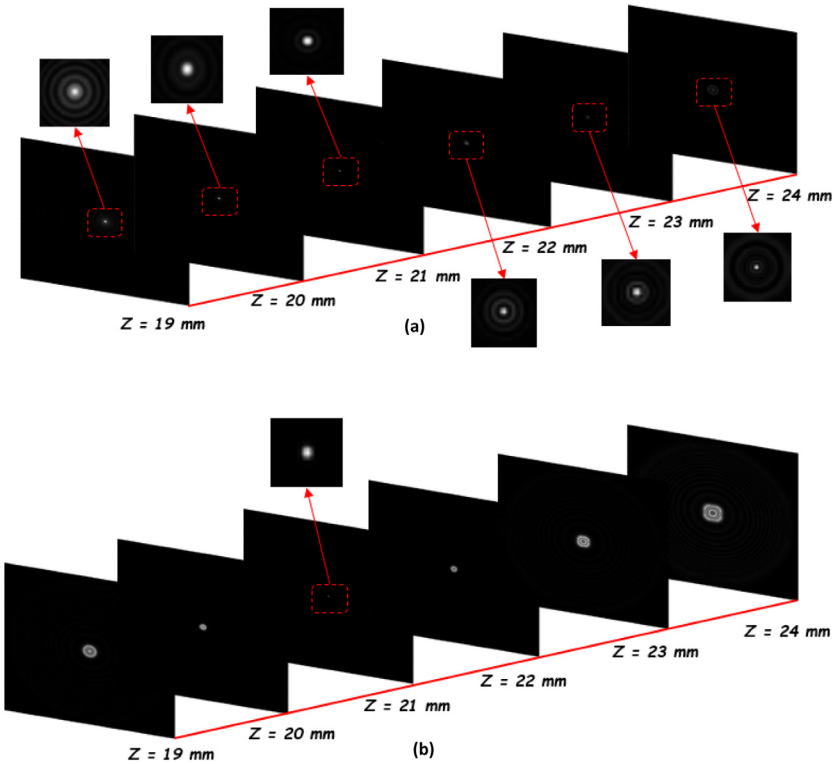

Fig. 6. Image simulation results: (a) EFZP and (b) FZP (see Visualization 1).

4. FABRICATION

During the fabrication process, direct laser lithography and a chemical etching process are applied to manufacture the final product. The entire process is presented in Fig. 8.

For the direct laser machine system, an EFZP pattern is required as input information. In other words, the laser path's movement must be generated by the traditional equation introduced in many previous studies [36–38]:

$$\sqrt{n\lambda f_m + \frac{n^2\lambda^2}{4}} = r_n. \tag{10}$$

Here r_n is the radius of the nth ring. To ensure that the acreage is similar, it is necessary for the outermost ring of each region to

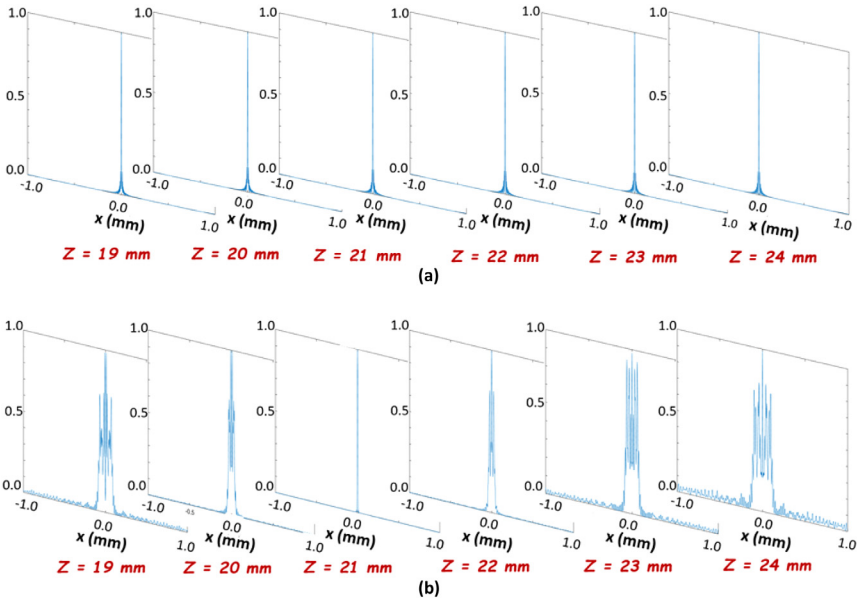

Fig. 7. Normalized intensity simulation result: (a) EFZP and (b) FZP (see Visualization 2).

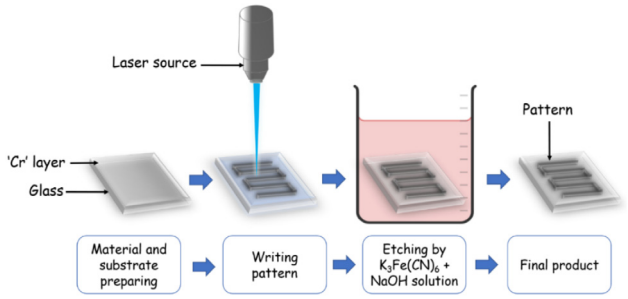

Fig. 8. Fabrication process.

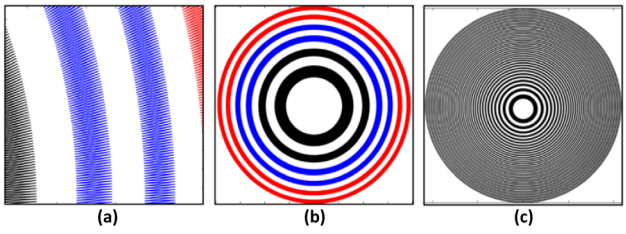

Fig. 9. (a) Laser moving path, (b) initial three regions of the EFZP, and (c) final pattern of the EFZP.

Table 2. EFZP Pattern Parameters

Region No.	f_m (mm)	n
1	20	1 to 4
2	20.1	5 to 8
3	20.2	9 to 12
4	20.3	13 to 16
5	20.4	17 to 20
6	20.5	21 to 24
7	20.6	25 to 28
8	20.7	29 to 32
9	20.8	33 to 36
10	20.9	37 to 40
11	21	41 to 44
12	21.1	45 to 48
13	21.2	49 to 52
14	21.3	53 to 56
15	21.4	57 to 60
16	21.5	61 to 64
17	21.6	65 to 68
18	21.7	69 to 72
19	21.8	73 to 76
20	21.9	77 to 80
21	22	81 to 84

have a similar value of $w \cdot \tau_m$, as shown in Table 1. The values for each parameter in Eq. (10) are provided in Table 2, with the wavelength λ set to 632.8 nm.

For every value of n, one r_n value is generated, and a pair of these values creates a ring, resulting in two rings in each region. Figure 9 illustrates the formation of the EFZP and the zig-zag pattern used to optimize the manufacturing process [39].

In the next step, the direct laser lithography system uses a laser beam source to illuminate Cr material on a glass substrate with a refractive index of approximately 1. Under the effect of the laser beam, the material turns to Cr_2O_3. In the following stage, a chemical treatment is utilized with two solutions—$K_3Fe(CN)_6$ and NaOH—for 5 min. Subsequently, the Cr is removed, while the Cr_2O_3 remains on the glass. In other words, the EFZP is successfully created. The detailed measurement results of the EFZP are shown in Fig. 10.

5. EXPERIMENTAL RESULTS

An optical verification system was designed to evaluate the effectiveness of the EFZP, as shown in Fig. 11. The system uses a He–Ne laser as a beam source with a wavelength of 632.8 nm. In order to reduce the intensity to suit the CMOS camera, a filter is used along with two lenses to expand the

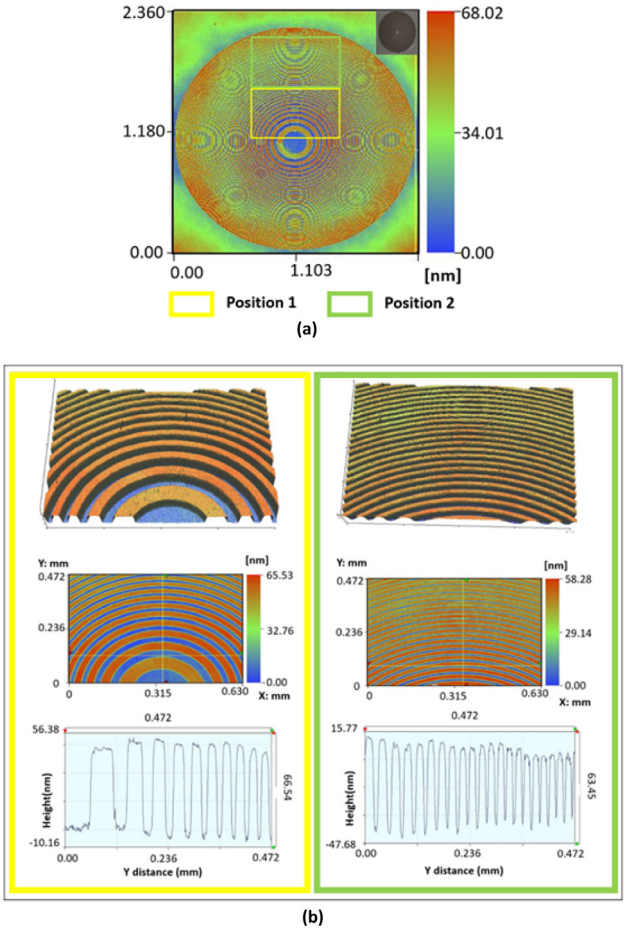

Fig. 10. (a) EFZP surface, where $R_a = 14.03$ nm, $R_q = 16.52$ nm, $R_t = 70.52$ nm, and $R_z = 70.27$ nm. (b) Measurement of two different areas of the EZP specimen: (a) Position 1 and (b) Position 2.

laser beam. Two lenses in the experiment are the Thorlabs AC254-030-A-ML ($f = 30$ mm, $D = 25.4$ mm, BBARR COATING 400–700 nm, N-BAF10/N-SF6HT) and Thorlabs AC254-300-A-ML ($f = 300$ mm, $D = 25.4$ mm, BBARR COATING 400-700 nm, N-BK7/SF2).

The CMOS camera is placed on a moving stage and travels a distance of 17–25 mm away from the zone plate. It should be noted that no other equipment is capable of enhancing the performance of the zone plate, meaning that the experimental results are the true representation of the EFZP. The results of the experiment are presented in Figs. 12 (see Visualization 3 for more detail) and 13. It is readily apparent that the outcome demonstrates a high level of agreement with the simulation results in the previous section.

The effective focal length ranges from 19 to 24.5 mm (5.5 mm) in comparison to the normal FZP, which ranges from 20.7 to 21.3 mm (0.6 mm). This implies that the depth of field has increased by approximately nine times. Figure 14 compares the focal spot diameter between the EFZP and normal FZP. On the one hand, the focal spot diameter of the EFZP remains consistent at approximately 0.035–0.04 mm throughout the 5.5 mm DoF. On the other hand, the focal spot diameter of the normal FZP is roughly 0.03 mm within the 0.6 mm DoF. Table 3 presents the results of a comparison of devices in previous research and the EFZP here.

6. CONCLUSION

In this research, a new method for creating an EFZP using direct lithography has been developed. The EFZP is based on the idea of a multi-region FZP, which can increase the DoF, depending on the number of regions and the focal length. A simulation is conducted using Fresnel propagation on Matlab software. The EFZP is then created using direct laser lithography and chemical etching on a glass substrate with a refractive index of approximately 1.

The optical verification system confirms that the EFZP closely matches the simulation. The EFZP can extend the DoF without the need for additional optical elements such as lenses or a SLM. The design of the EFZP is highly flexible and can be adjusted for different purposes by changing parameters such

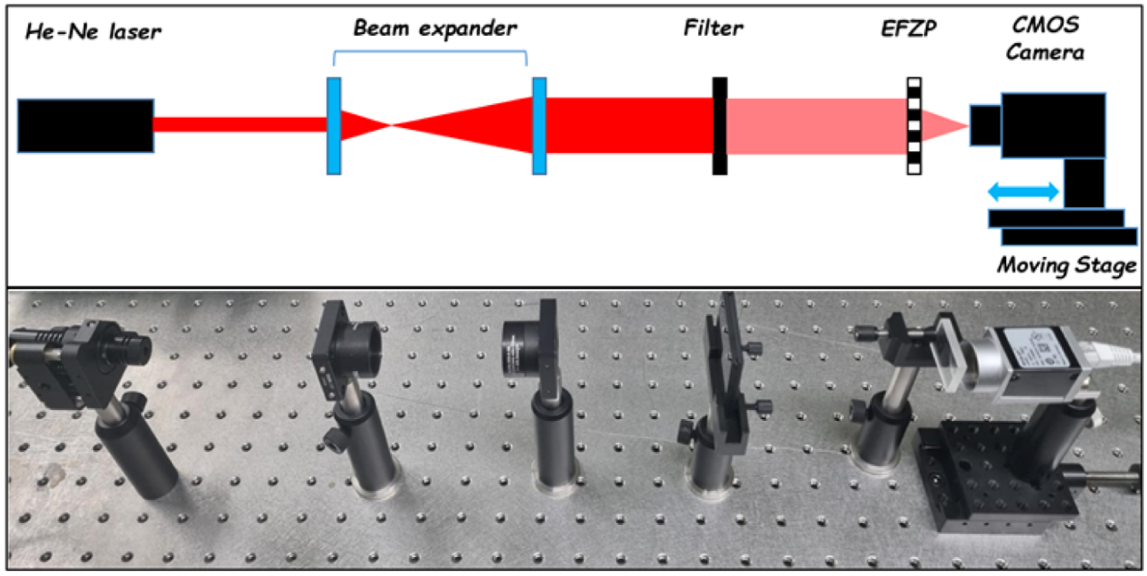

Fig. 11. Experimental setup.

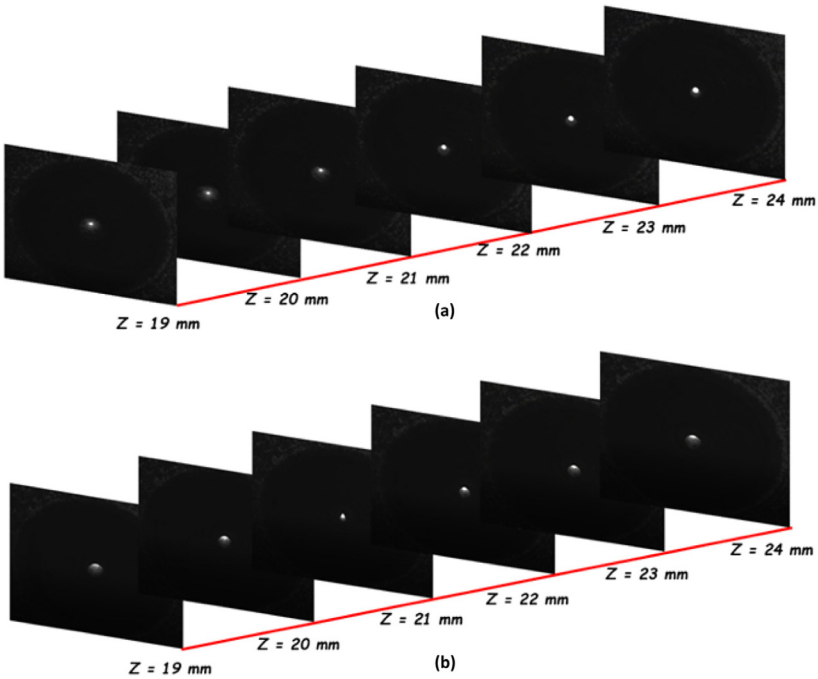

Fig. 12. Experiment image results: (a) EFZP and (b) FZP (see Visualization 3).

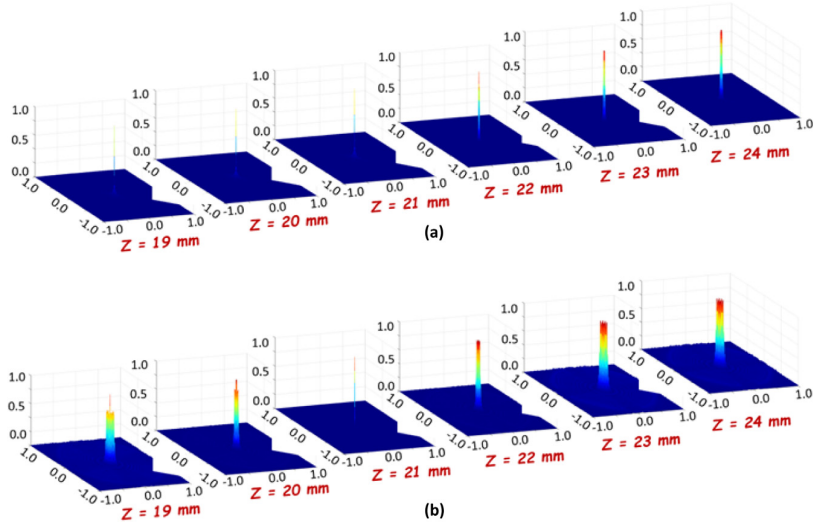

Fig. 13. Experiment intensity results: (a) EFZP and (b) FZP.

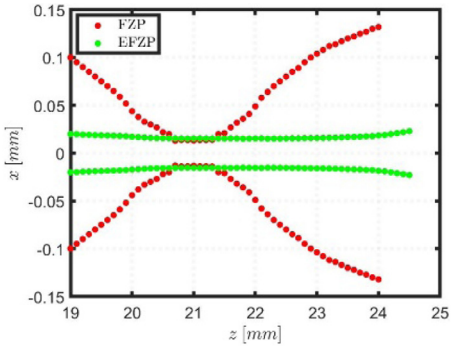

Fig. 14. Focal spot diameter comparison.

as the number of regions, their size, or the order of the focal lengths.

This new concept has several advantages over those presented in previous studies. First, it eliminates the need for support equipment such as lenses or a SLM, reducing both the cost and size of the system, while also removing optical aberrations. Additionally, the design of the EFZP minimizes the opaque area, unlike a fractal zone plate. This makes it a viable option for applications in microscopy, coherence tomography, and direct lithography, particularly in UV and X-ray band imaging, where the use of lenses is difficult and the depth of field is crucial. Furthermore, the EFZP can function as a filter if the wavelength value λ differs in certain regions. In future work, we plan to

Table 3. Comparison Results

Concept	DoF (mm)	Extend DoF	Note
Fractal Zone plate [14]	2.5	14 times greater	Require lenses
Quasi-fractal zone plate [15]	20	1.5 times greater	Require a special image device to achieve a better result
Sector-based zone plate [16]	25	5 times greater	Require two lenses, a pin hole, and a SLM to create a sector-based Zone plate
Multi-ring pure-phase binary optical elements [17]		2.5	Require a lens and a SLM
EFZP	***5***	***9 times greater***	***Support equipment is no required.***

develop a method for optimizing the intensity and focal spot diameter of this EFZP to improve its performance.

Funding. Ministry of Trade, Industry and Energy (MOTIE, Korea) (1415187786, RS-2023-00237714, 20020311).

Acknowledgment. All authors contributed to the study conception and design. Material preparation, data collection, and analysis were performed by Hieu Tran Doan Trung, Hai Linh Vu Nguyen, Atar Munnibee, Young-Jin Kim, YoungShik Ghim, and Hyug Gyo Rhee. The first draft of the manuscript was written by Hieu Tran Doan Trung, and all authors commented on previous versions of the manuscript. All authors read and approved the final manuscript.

Disclosures. The authors declare no conflicts of interest.

Data availability. Data underlying the results presented in this paper are not publicly available at this time but may be obtained from the authors upon reasonable request.

REFERENCES

1. X. Zhang, X. Liu, and X. Chen, "Computer-generated holograms for 3D objects using the Fresnel zone plate," Proc. SPIE **5636**, 5704–5712 (2005).
2. Z. Sun, X. Sang, C. Zhong, *et al.*, "Real-time interactive computer-generated hologram using Fresnel zone plate extension method," Proc. SPIE **12318**, 2643–2663 (2022).
3. H. Zheng, F. Wu, T. Sun, *et al.*, "Imaging quality analysis of computer generated holograms in 3D holographic display using different Fresnel zone plates in look-up table," Proc. SPIE **9524**, 677–682 (2015).
4. D. Alexandre, A. P. Louisa, J. K. Bernard, *et al.*, "Fresnel zone plate development for x-ray radiography of hydrodynamic instabilities at the National Ignition Facility," Appl. Opt. **59**, 785–10777 (2020).
5. J. Soltau, P. Meyer, R. Hartmann, *et al.*, "Full-field x-ray fluorescence imaging using a Fresnel zone plate coded aperture," Optica **10**, 127–133 (2023).
6. B. Macdonald, L. T. Chang, V. Perez-Mendez, *et al.*, "Gamma-ray imaging using a Fresnel zone plate aperture," IEEE Trans. Nucl. Sci. **21**, 678–684 (1974).
7. H. H. Barrett and F. A. Horrigan, "Fresnel zone plate imaging of gamma rays, theory," Appl. Opt. **12**, 2686–2702 (1973).
8. J. Kirz, "Phase zone plates for x rays and the extreme u," J. Opt. Soc. Am. **64**, 301–309 (1974).
9. V. A. Baez, "Fresnel zone plate for optical image formation using extreme ultraviolet and soft x radiation," J. Opt. Soc. Am. **51**, 405–412 (1961).
10. L. J. Huang, G. M. Zhang, H. Li, *et al.*, "Selective laser ablation and patterning on Ag thin films with width and depth control," J. Mater. Sci. **31**, 4943–4955 (2020).
11. X. Sun, Q. Zou, H. Zhou, *et al.*, "LIBS repeatability study based on the pulsed laser ablation volume measuring by the extended depth of field microscopic three-dimensional reconstruction imaging," Opt. Lasers Eng. **153**, 107003 (2022).
12. S. Liu and H. Hua, "Extended depth-of-field microscopic imaging with a variable focus microscope objective," Opt. Express **19**, 353–362 (2011).
13. S. Jaroslaw, M. Michal, K. Andrzej, *et al.*, "Extended depth of focus for high-end machine vision lenses by annular achromatic add-on diffractive elements," Opt. Lasers Eng. **162**, 107445 (2023).
14. Q. Q. Zhang, J. G. Wang, M. W. Wang, *et al.*, "A modified fractal zone plate with extended depth of focus in spectral domain optical coherence tomography," J. Opt. **13**, 055301 (2011).
15. Q. Q. Zhang, J. Wang, M. Wang, *et al.*, "Depth of focus enhancement of a modified imaging quasi-fractal zone plate," Opt. Laser Technol. **44**, 21402144 (2012).
16. N. Xu, Z. Kong, Q. Tan, *et al.*, "Multiring pure-phase binary optical elements to extend depth of focus," Appl. Opt. **57**, 9643–9648 (2018).
17. F. J. Torcal-Milla, L. M. Sanchez-Brea, and J. A. Gomez-Pedrero, "Sector-based Fresnel zone plate with extended depth of focus," Opt. Laser Technol. **154**, 108294 (2022).
18. J. Liu, P. Jiang, H. Yang, *et al.*, "Multi-focus composite spiral zone plate to generate focused vortices with the comparable intensity based on genetic algorithm," Opt. Express **31**, 35363–35376 (2023).
19. T. Liu, Q. Liu, S. Yang, *et al.*, "Shaping a far-field optical needle by a regular nanostructured metasurface," Opt. Commun. **393**, 72–76 (2017).
20. C. Han, Y. Tang, X. Cheng, *et al.*, "A novel coaxial focus position detection technique based on differential modulation evaluation for laser direct photolithography," Opt. Lasers Eng. **161**, 107396 (2023).
21. J. Cunha, I. S. Garcia, J. D. Santos, *et al.*, "Assessing tolerances in direct write laser grayscale lithography and reactive ion etching pattern transfer for fabrication of 2.5D Si master molds," Micro Nano Eng. **19**, 100182 (2023).
22. C. A. Rothenbach and M. C. Gupta, "High resolution, low cost laser lithography using a Blu-ray optical head assembly," Opt. Lasers Eng. **50**, 900–904 (2012).
23. N. H. A. Nguyen, H. Rhee, and Y. S. Ghim, "Novel fabrication and designs for hybrid optical elements with wider angle field of view by using integrated direct laser lithographic system," Opt. Lasers Eng. **170**, 107774 (2023).
24. N. H. A. Nguyen, H. Rhee, P. Kang, *et al.*, "Design and fabrication of an off-axis elliptical zone plate in visible light," Curr. Opt. Photonics **6**, 44–50 (2022).
25. N. H. A. Nguyen, H. Rhee, and Y. S. Ghim, "Design and lithographic fabrication of elliptical zone plate array with high fill factor," Curr. Opt. Photonics **5**, 8–15 (2021).
26. R. Grella, "Fresnel propagation and diffraction and paraxial wave equation," J. Opt. **13**, 367 (1982).
27. T. W. Rhodes, "Numerical simulation of Fresnel-regime wave propagation: the light-tube model," Proc. SPIE **4436**, 451302 (2001).
28. S. Hrivňak, J. Uličný, and P. Vagovič, "Fast Fresnel propagation through a set of inclined reflecting planes applicable for X-ray imaging," Opt. Express **26**, 34569–34579 (2018).
29. D. G. Voelz, *Computational Fourier Optics: A MATLAB Tutorial* (2011), Vol. **TT89**, p. 110.
30. D. G. Voelz, *Computational Fourier Optics: A MATLAB Tutorial* (2011), Vol. **TT89**, p. 53.
31. D. G. Voelz, *Computational Fourier Optics: A MATLAB Tutorial* (2011), Vol. **TT89**, p. 49.
32. T. Liu, J. Wang, Q. Liu, *et al.*, "Chromatic confocal measurement method using a phase Fresnel zone plate," Opt. Express **30**, 2390–2401 (2022).

33. T. Liu, Q. Liu, S. Yang, *et al.*, "Investigation of axial and transverse focal spot sizes of Fresnel zone plates," Appl. Opt. **56**, 3725–3729 (2017).
34. Q. Liu, T. Liu, S. Yang, *et al.*, "Axial intensity distribution of a micro-Fresnel zone plate at an arbitrary numerical aperture," Opt. Express **29**, 12093–12109 (2021).
35. S. Xue, Q. Liu, T. Liu, *et al.*, "Electromagnetic exploration of focusing properties of high-numerical-aperture micro-Fresnel zone plates," Opt. Commun. **426**, 41–45 (2018).
36. Q. Zhang, Q. Fan, Z. Yang, *et al.*, "Toward binary Gabor zone plate by modulating zones width," Optik **174**, 387–393 (2018).
37. D. C. Calvo, A. L. Thangawng, M. Nicholas, *et al.*, "Thin Fresnel zone plate lenses for focusing underwater sound," Appl. Phys. Lett. **107**, 014103 (2015).
38. J. M. Fuster, S. Pérez-López, P. Candelas, *et al.*, "Design of binary-sequence zone plates in high wavelength domains," Sensors **18**, 2604 (2018).
39. N. H. A. Nguyen, H. Rhee, Y. S. Ghim, *et al.*, "Novel fabrication process for an array of elliptical zone plates by using direct laser lithography," Int. J. Adv. Manuf. Technol. **106**, 2629–2634 (2020).